

LBONet: Supervised Spectral Descriptors for Shape Analysis

Oguzhan Yigit, Richard C. Wilson, *Senior Member, IEEE*

Abstract—The Laplace-Beltrami operator has established itself in the field of non-rigid shape analysis due to its many useful properties such as being invariant under isometric transformation, having a countable eigensystem forming an orthonormal basis, and fully characterizing geodesic distances of the manifold. However, this invariance only applies under isometric deformations, which leads to a performance breakdown in many real-world applications. In recent years emphasis has been placed upon extracting optimal features using deep learning methods, however spectral signatures play a crucial role and still add value. In this paper we take a step back, revisiting the LBO and proposing a supervised way to learn several operators on a manifold. Depending on the task, by applying these functions, we can train the LBO eigenbasis to be more task-specific. The optimization of the LBO leads to enormous improvements to established descriptors such as the heat kernel signature in various tasks such as retrieval, classification, segmentation, and correspondence, proving the adaption of the LBO eigenbasis to both global and highly local learning settings.

Index Terms—spectral descriptor, Laplace-Beltrami operator, Isospectralization.

I. INTRODUCTION

SHAPE analysis has been greatly affected by the recent introduction of deep learning techniques, resulting in numerous papers on the incorporation of machine learning methods in shape analysis tasks. When looking at these papers chronologically, we can see that the state-of-the-art is a result of accumulative work. Most of the classical supervised and unsupervised learning methods are based on Euclidean data. However, graphs and Riemannian manifolds which represent shape are non-Euclidean, we cannot directly apply these methods to them. Hence, the primary focus of research in shape analysis in recent years was to find analogies of these methods in the non-Euclidean domain, such as the *patch* operator [1], supervised bag of visual words [2], and non-Euclidean convolution [3]. These efforts led to the successful application of convolutional neural networks and deep learning techniques on manifolds, both in the spatial and spectral domain. Both domains have their unique features, but a significant drawback of spectral CNNs has always been the lack of generalization across manifolds, even though techniques, such as synchronized Spectral CNN [4] were introduced to overcome this.

Almost forgotten by the focus on global encoding techniques, recent frameworks PointNet++ [5], second-order spec-

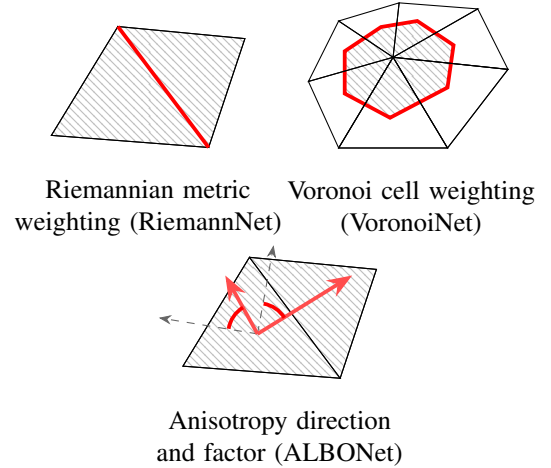


Fig. 1. LBONet comprises multiple modules which operate directly on the input mesh. RiemannNet is able to weight Riemannian metric on a manifold, ALBONet introduces anisotropy by rotating and factoring the diffusion speed, and lastly VoronoiNet weights the Voronoi cells. These affect the Laplace-Beltrami operator in several different ways, allowing the operator to adapt to the given data and alleviate the performance breakdowns incurred by non-isometric deformations.

tral transform [6], DiffusionNet [7] demonstrate the continuing importance of spectral descriptors for non-rigid shape analysis, where a significant increase of accuracy is achieved on challenging benchmarks by using spectral descriptors as opposed to using only geometric properties such as point coordinates.

Although the performance gain using spectral descriptors is becoming less as recent works have shown. The presented work can be plugged in any existing pipeline making use of spectral descriptors and promises to achieve further gains, which could make all spectral-based methods more attractive in the wider literature. This not only proves the capability of feature retrieval networks to make use of spectral descriptors, but also their descriptive power. Deep learning methods slowly superseded dictionary-based retrieval methods such as bag of words [2] or Fisher and Super Vector [8], due to their ease of use and end-to-end learning capability, however it is still not clear how they compare to those methods since [9] [10] [11] have shown good performance in common benchmarks. Many papers have been published on modifying the LBO eigenbasis [11] [12] [13], but very few papers dedicate themselves learning through the LBO eigenbasis. Some attempts have been made recently such as HodgeNet [14], but competing methods have overcome them quickly. However backpropagating through the LBO eigendecomposition remains challenging and despite dealing with sparse matrices the backpropagation

Oguzhan Yigit and R. C. Wilson are with Department of Computer Science, University of York, UK. E-mail: oguzhan.yigit@york.ac.uk, richard.wilson@york.ac.uk

Code available online under <https://github.com/yioguz/LBONet>

involves dense matrices, which in turn introduce problems with scalability. This work introduces custom PyTorch routines to deal with the given inherent sparsity of the data, to speed up the backpropagation, allowing to process high resolution data in a reasonable timeframe.

This paper takes an unconventional way and dedicates itself on how learning can be enabled through the LBO eigenbasis, in order to improve spectral descriptors and to make them more task-specific.

As demonstrated by this work spectral methods can beat state-of-the-art methods after weighting the LBO accordingly. The learned weights roughly reflect the task at hand, e.g. in a segmentation task, boundary regions express increased activity, whereas in a correspondence tasks, near-isometric deformations on the manifold express increased activity, making it easier for descriptors or mlps to pickup the right details from the spectral descriptor. The intriguing question this paper tackles is how much learning potential is hidden in the LBO eigenbasis, how much of it can be exploited, and what are the limiting factors to achieve further performance gains.

These performance gains are achieved by introducing weighting layers, which we call modules in the following, which weight the manifold in different ways and modify the nature of the LBO. In prior work it was not possible to learn them with backpropagation and methods have either used heuristics or precalculation of many combinations of parameters. Learning these modules offers more advantages over the traditional methods as the learning can learn complex non-linear relationships in the data and is not restricted by predefined values.

The ablation study shows that LBONet is able to outperform some methods by just weighting the LBO and producing a spectral descriptor. It produces competitive results, when paired with a backend, which utilizes the gains of LBONet.

Contributions We present an end-to-end learning framework for learning operators on triangle meshes to improve the performance of spectral descriptors. With the introduction of our framework we make the following contributions,

- a learnable block which learns a Riemannian metric weighting layer based on intrinsic shape features
- a learnable block which learns Voronoi cell weighting layer based on intrinsic shape features;
- a learnable block which learns an anisotropic LBO (ALBO) layer based on intrinsic shape features and optionally into two directions (ALBO+)
- a modern backpropagation implementation for differentiating eigenderivatives in PyTorch, which exploits the the sparsity of the data and addresses only as few eigenfrequencies as set;
- an end-to-end approach for learning, starting from features on the mesh up to the descriptor;

II. BACKGROUND

a) *Laplace-Beltrami Operator*: The Laplace-Beltrami operator (LBO) is the generalization of the Laplace operator

onto Riemannian manifold M and given f , a real-valued function with $f \in C^2$, it is defined as:

$$\Delta f = \text{div}(\nabla f), \quad (1)$$

where ∇f is the gradient of f and div the divergence on the manifold. It was introduced first into shape analysis with ShapeDNA [15]. It utilizes the eigenvalues of the operator on a manifold to form an invariant embedding.

Spectral Theorem The LBO is a self-adjoint, semi-positive definite operator and therefore admits an orthonormal eigen-system, which can be retrieved by solving the eigenvalue problem:

$$\Delta \phi_k = \lambda_k \phi_k, \quad (2)$$

where λ_k and ϕ_k is the corresponding pair of eigenvalue and eigenvector, respectively. As we deal with discrete approximations of manifolds such as meshes, point clouds, and voxels, we need to discretize the LBO. Several discretization methods have been proposed for triangle meshes, but the cotangent weight method [16] has established itself, and is defined as:

$$\Delta f = Lf = A^{-1}Wf, \quad (3)$$

where L denotes the discrete Laplacian, and W is referred to as *stiffness matrix* and its elements are defined by:

$$W(i, j) = \begin{cases} \frac{\cot \alpha_1 + \cot \alpha_2}{2}, & \text{if } (i, j) \in E \\ -\sum_{k \neq i} W(i, k), & \text{if } i = j \\ 0, & \text{otherwise,} \end{cases} \quad (4)$$

α_1 and α_2 are the opposing angles in an edge flap, which is depicted in figure 4. A is referred to as *mass matrix* and is a diagonal matrix and is composed of the area of the *Voronoi* cell,

$$A(i, j) = \begin{cases} \frac{1}{8} \sum_{j \in N_1(i)} (\cot \alpha_1 + \cot \alpha_2) \|d_{ij}\|^2, & \text{if } i = j \\ 0, & \text{otherwise,} \end{cases} \quad (5)$$

where d_{ij} denotes the distance between vertex i and j , and $N_1(i)$ is the one-ring neighbourhood of vertex i (see figure 7). Another popular choice for the mass matrix is using barycentric cells [7] [17]. Finally, we derive the generalized eigenvalue problem:

$$W\phi = \lambda A\phi. \quad (6)$$

Following ShapeDNA's [15] example, Rustamov [18] introduced the global point signature (GPS), which is defined at vertex i as,

$$GPS(i) = \left(\frac{1}{\sqrt{\lambda_1}} \phi_1(i), \frac{1}{\sqrt{\lambda_2}} \phi_2(i), \dots, \frac{1}{\sqrt{\lambda_n}} \phi_n(i) \right), \quad (7)$$

where n defines the upper boundary for the eigensystem. Despite being the first signature making use of the full spectrum of the LBO, it suffered from several drawbacks such as the flipping of eigenvectors due to said eigenvectors being defined only up to a sign and swapping of eigenvectors. Motivated by aforementioned drawbacks, Sun *et al.* [19] introduced a signature based on the heat diffusion process, which is still

relevant in most shape analysis methods. The heat diffusion process is given by

$$\Delta f(i, t) = -\frac{\partial f(i, t)}{\partial t}, \quad (8)$$

where $f(x, t)$ is the temperature at point i at time t . By the *informative theorem* [19], the heat kernel can be expressed in the spectral domain by restricting it to the diagonal elements:

$$h_t(i, i) = \sum_{k>0} e^{-t\lambda_k} \phi_k(i)^2. \quad (9)$$

As the heat kernel varies with the scale of a manifold, which can cause some performance breakdowns, a scale-invariant variant version was proposed by Bronstein *et al.* [20].

III. RELATED WORK

As the term *spectral methods* is used interchangeably for methods based on spectral descriptors and methods which aim to improve the underlying LBO by changing its characteristics, it is crucial to draw a contrast between them since they tackle the same problem in completely different ways. In the following, we therefore refer to those methods based on spectral descriptors as *spectral methods* and to methods which manipulate the behaviour of the underlying LBO as *LBO methods*.

A. Spectral Methods

The introduction of the heat and wave kernel signature have spawned a plethora of methods in an attempt to overcome the downsides of spectral descriptors. Though the downsides are inherent to the underlying LBO, some can be mitigated by learning based on the spectral descriptors. There are heuristic methods which optimize the hyperparameters of these signatures such as scaling the eigenvalues in improved wave kernel signature [8] or optimizing the variance parameter in the wave kernel signature [21]. Litman *et al.* parameterize spectral descriptors [22] and make it possible to systematically learn an optimal signature by metric learning. Other methods on the other hand rely completely on the descriptive power of spectral descriptors and learn with an elaborate feature retrieval network. PointNet++ [5] introduced a novel method to consume point clouds and applied it to the non-rigid domain by using spectral descriptors and geometric features as input. Second-order spectral transform [6] employed second-order pooling on spectral descriptors and based their learning on top of the second-order pooled descriptor and learn on the resulting SPDM-manifold. They achieve moderate results on SHREC'15 but achieve unparalleled performance on the challenging SHREC'14 human benchmarks, which to the best of our knowledge, is outperformed only by the presented method. Dynamic graph convolutional neural network [23] constructs a local neighborhood graph and learns a neighbourhood function, allowing the sharing of information across k-nearest neighbours, thereby adding an additional layer for learning. DiffusionNet [7] takes optionally spectral descriptors as input features and applies spatially shared mlps on a feature construct, but does not learn in the spectral domain itself.

B. LBO Methods

As the downsides of spectral signatures are inherent to the LBO, the question arises: to what degree can these downsides be compensated for by modifying the nature of the LBO. The kinetic Laplace-Beltrami operator [11] achieves significant boost of performance by weighting the mass matrix with a kinetic energy term derived from the curvature of the manifold. Similarly, the Hamiltonian [12] operator applies an optimized potential V to the spectrum and thus changes the behaviour of the LBO by modifying the diagonal entries of the stiffness matrix using perturbation theory.

As there was no straightforward way to backpropagate through the LBO eigenbasis, methods either relied on heuristics or precalculation with a set of different parameters such as anisotropic diffusion descriptors [24] or anisotropic convolutional neural network [25]. Another intriguing extension of the ALBO is the FLBO [26], which removes the quadratic assumption of the Riemmanian metric, allowing asymmetries on the manifold.

Some methods however attempted successfully to backpropagate through the LBO eigenbasis, one of which is [27], where a shape is iteratively optimized wrt. the eigenvalues of a target shape and then is used in follow up tasks such as finding correspondences between these "isospectralized" shapes. Isospectralization is a concept, which aims to reduce the spectral distance of shapes as much as possible eventually resulting in a similar spectrum, hence the coined term Isospectralization. A similar work has been presented in [28], where this concept has been incorporated to Hamiltonian spectrum and partial shapes. Although isospectralization is an effective tool, recent works achieve high accuracies in correspondence tasks with higher degrees of non-isometry, proving that correspondences can be learnt even if the eigenbasis is not aligned. The presented work can also be seen as a part of Isospectralization, as LBONet aims to a task-specific LBO eigenbasis, which in a correspondence setting leads to a spectrum, which is as close as possible to similar manifolds. As the experiments show, Isospectralization is only one of many things LBONet is able to achieve. In a segmentation task it is able to spread the segmented parts in the spectrum. Furthermore, the presented work operates on both levels eigenvalues and eigenvectors.

The methods introduced by conformal metric optimization on surfaces [29] and Riemannian metric optimization on surfaces [17], despite their limited application to intrinsic brain mapping, have been groundbreaking as they form the first rudimentary end-to-end optimization of spectral descriptors. In the former, the authors optimize the mass matrix, whereas in the latter, the authors optimize the Riemannian metric, which translates to optimizing both, stiffness and mass matrix. More recently, HodgeNet [14] follows the same goal of learning end-to-end by backpropagating through the eigenbasis of the *Laplace-Beltrami* operator by approximating the gradients wrt. Hodge star operators.

The presented paper instead calculates the exact gradients, which do not require the calculation of additional eigenvectors such as in [14]. Furthermore, it introduces several learning operators, which were previously only based on heuristics or

precalculation, and allows to learn optimal weights for a given dataset.

IV. APPROACH

A. Building blocks

The following approach is based on the fact that any non-isometric deformation distorts the LBO eigenbasis drastically. This can be illustrated by using functional maps [30], where the C matrix, which maps the eigenbases on one manifold to another, deviates from the diagonal matrix with even mild near-isometries. The greater the non-isometric deformation, the further the map deviates from the diagonal, making the map more complex and less sparse and due to this fact the LBO eigenbasis become less ideal as a basis function. This effect is illustrated in figure 2, with an intra-class manifold for near-isometry and an inter-class manifold for non-isometry. This sensitivity and instability of the LBO eigenbasis intro-

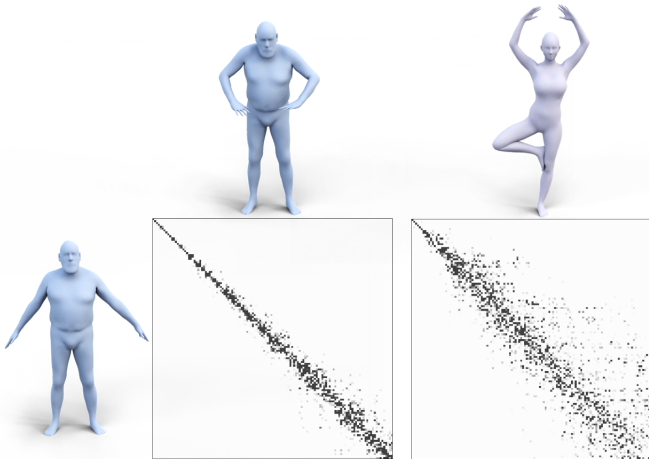


Fig. 2. Functional matrix between an intra-class manifold pair (left yellow and top yellow) and a inter-class manifold pair (left yellow and top turquoise). One can observe two things, first, the functional matrix deviates from the diagonal even with mild non-isometries and second, that with greater deformation, the matrix deviates even further.

duces two drastic downsides, firstly, it makes it difficult to transfer features learnt in the spectral space and, secondly, the overlying descriptor needs to span the spectral range a manifold can be embedded in, which could lead to a less precise descriptor.

To alleviate this, learning can be done both implicitly and explicitly. Implicit learning would learn an optimal descriptor based on the LBO eigenbasis and learning thereby only implicitly an ideal LBO eigenbasis, e.g. for a segmentation task, the learning can be done on the heat kernel directly, which then propagates the loss back to the eigenbasis. Whereas explicit learning would learn an LBO eigenbasis directly from the loss function and the loss would be given directly on the LBO eigenbasis, e.g. in a correspondence task, we might learn the eigenbasis directly, rather than going via an overlying descriptor.

The presented approach and experiments are all done by learning the LBO eigenbasis implicitly. Learning the LBO eigenbasis explicitly is beyond the scope of the presented paper and is subject to further research.

We give the gradients below in the context of learning through the heat kernel signature, but they can be analogously derived for any other spectral signature such as the wave kernel signature [31] or average mixing kernel signature [32]. With the given loss LBONet takes the aim to weight the LBO s.t. the produced eigenbasis and the descriptor is better at the given task. Weighting the LBO is a common practice and as described in the related work sections used quite effectively in various tasks. However, as the backpropagation through the LBO eigenbasis is a challenging task, hyperparameters could not be learned easily and were therefore based on heuristics. We show the weighting based on three different elements, which are depicted in gray in figure 3. Firstly, by using features on mesh edges to weight the Riemannian metric (RiemannNet), which by default is defined as the edge length of the mesh. Secondly, on faces, by adjusting the anisotropy (ALBONet), and lastly using features on vertices to weight the Voronoi cell (VoronoiNet).

We equip each block with EdgeConv which creates a local neighbourhood graph as in [23] and learns a neighbourhood function. This allows the sharing of information in the local neighborhood and to learn more effectively generalizing features. This proved far superior to learning directly from the features only sourcing their information from the local context. As a distance function, Euclidean distance showed good performance, although in some cases constructs neighbourhood erroneously, e.g. when a disjoint body part such as a hand is close to the hip, the hip might exchange information with the hand. We observed some downside effect in the experiments, however, the drawback was negligible, hence we omitted the construction of a geodesic neighborhood.

These features are then passed through multiple shared mlps to predict the Riemannian metric weighting, which can shorten or expand distances on specific regions by scaling the Riemannian metric, steer the anisotropy individually on each face by rotating the orthogonal principal curvature basis and scaling the anisotropic factors, and finally weight the Voronoi cell differently across the manifold. These predictions are applied directly on the discretized LBO, modifying the stiffness L and mass matrix A in various ways, which we detail out from subsection D onwards. This modified LBO eigenbasis $(\hat{\lambda}, \hat{\phi})$ is then used to evaluate a spectral descriptor, which then can be either passed into a "backend" (see figure 3 for further processing or used directly for various tasks.

B. Feature Learning

Works on learning from unordered point clouds such as in PointNet [33], PointNet++ [5], and DGCNN [23] or spectral methods such as Spectral Transform Block [6] proved useful for shape analysis tasks. More recently point (cloud) transformers [34] [35] and the heat kernel based transformer [36] have further pushed the boundaries in extracting powerful features.

In particular, their performance in non-rigid shape analysis using spectral descriptors rather than point coordinates proves that they are able to utilize the information within spectral descriptors, and furthermore, that there is still unexploited

potential in them, as the standard LBO is not invariant under non-isometric deformation. The presented work explores to what extent spectral descriptors can contribute to the descriptiveness of features when using state-of-the-art feature extracting networks, by putting as much learning as possible into the spectral descriptor and the LBO eigenbasis. We highlight the tradeoffs of this level of adaption of the LBO to the given task in the conclusion.

1) *Edge-, Face-, Vertexwise Perceptrons*: With the propagated loss through the LBO eigenbasis, we can learn features from mesh edges by RiemannNet, from mesh faces by ALBONet and from mesh vertices by VoronoiNet. For this we use the concept of shared mlps, which has been used widely in the literature and been referred to as *-wise perceptrons. Furthermore, experiments have shown that EdgeConv introduced by [23] yielded an additional performance gain. For edges and faces, we take the mean of their coordinates to build a coordinate system to find the nearest neighbours and use the asymmetric edge function given by [23],

$$h_{\Theta}(x_i, x_j) = h_{\Theta}(x_i, x_j - x_i). \quad (10)$$

followed by several shared mlp layers.

2) *Input Features*: As input to our pipeline we use intrinsic shape features derived from the second fundamental form such as mean curvature [37], gaussian, shape index, curvature index. For faces and edges we interpolate the features from their vertices. The intention is to limit the input features to intrinsically invariant features to avoid any dependency on the shape embedding and also have robust features, which are mostly independent from the meshing structure and resolution.

Usage of point coordinates as input features could yield an additional benefit, however at the cost of extensive training. Furthermore, intrinsic shape features prove to be significant for non-rigid shape analysis as shown in [38] and are widely used as enhancing input features [5] [23] [7] for non-rigid shape analysis.

The predictions of the the modules (RiemannNet, ALBONet, and VoronoiNet) modify the stiffness and mass matrix in different ways, which then can be used to solve the generalized eigenvalue problem,

$$W\hat{\phi} = \hat{\lambda}A\hat{\phi} \quad (11)$$

resulting in a modified task-specific eigenbasis $(\hat{\lambda}, \hat{\phi})$.

C. Sensitivity Analysis of Spectral Descriptors

To learn an optimal LBO eigenbasis, one needs to differentiate the generalized eigenvalue problem (6) wrt. to any given parameter p :

$$\frac{\partial W}{\partial p_{ij}}\phi + W\frac{\partial \phi}{\partial p_{ij}} = \frac{\partial \lambda}{\partial p_{ij}}A\phi + \lambda\frac{\partial A}{\partial p_{ij}} + \lambda A\frac{\partial \phi}{\partial p_{ij}}. \quad (12)$$

Differentiating the stiffness W and mass matrix A is trivial, whereas the eigenbasis involves multiple steps. Nelson’s method [39] has established itself for differentiating eigenvalues and eigenvectors and has been used widely throughout the literature. For the mass matrix, rather than using barycentric cells as in [29] [17], we opt for using Voronoi cells introduced by [16], as they prove to be more robust to meshing structure

and is recommended by [16], due to having a provably tight error bound. Depending on whether the task at hand impacts the stiffness and/or mass matrix, Nelson’s method needs to be adjusted accordingly. In the following we demonstrate the default method, but make use of all variations of Nelson’s method, stiffness & mass matrix, stiffness only, and mass only in the following sections.

From equation 12 we obtain for eigenvalue λ_k ,

$$\frac{\partial \lambda_k}{\partial p_{ij}} = \phi_k^T (\Delta A - \lambda_k \Delta W) \phi_k, \quad (13)$$

and for eigenvector ϕ_k ,

$$\frac{\partial \phi_k}{\partial p_{ij}} = \mu_{ij} + c \phi, \quad (14)$$

where μ is the result of the following equation,

$$(W - A)\mu_{ij} = F_i, \quad (15)$$

and F_i is defined as,

$$F_i = \phi^T \left(\frac{\partial W_k}{\partial p_{ij}} - \lambda_i \frac{\partial A_k}{\partial d_{ij}} \right) \phi A \phi - \left(\frac{\partial W_k}{\partial p_{ij}} - \lambda_i \frac{\partial A_k}{\partial p_{ij}} \right) \phi \quad (16)$$

and c as

$$c = -\mu A \phi - \frac{1}{2} \phi^T \Delta A \phi. \quad (17)$$

With the eigenbasis gradients at hand, we can differentiate any given spectral descriptor, i.e. the heat kernel signature wrt. to any parameter p on a manifold M ,

$$\frac{\partial h_t}{\partial p_{ij}} = \sum -te^{-\lambda t} \phi^2 \frac{\partial \lambda}{\partial p_{ij}} + 2e^{-\lambda t} \phi \frac{\partial \phi}{\partial p_{ij}} \quad (18)$$

which allows us to do an end-to-end analysis, back propagating the loss from the spectral descriptor down to the individual parameter.

D. Learning on mesh edges

Having established the groundwork, we move on setting up the parameters we want to learn on a manifold and first approach learning the Riemannian metric g , which by default is defined on the mesh edge as its length d_{ij} . For this we inherit the gradients for the stiffness matrix W from [17], but introduce the gradients for the mass matrix A using Voronoi cells in the following. As the following gradients are similar in nature, we demonstrate them by giving one example and refer the reader to the supplementary materials for detailed gradients and their derivation, which are all derived by basic calculus.

Adjusting any given Riemannian metric has an impact on the surrounding edge flap and thus angles and distances change within this edge flap and the gradients for RiemannNet are derived from the components depicted in figure 4.

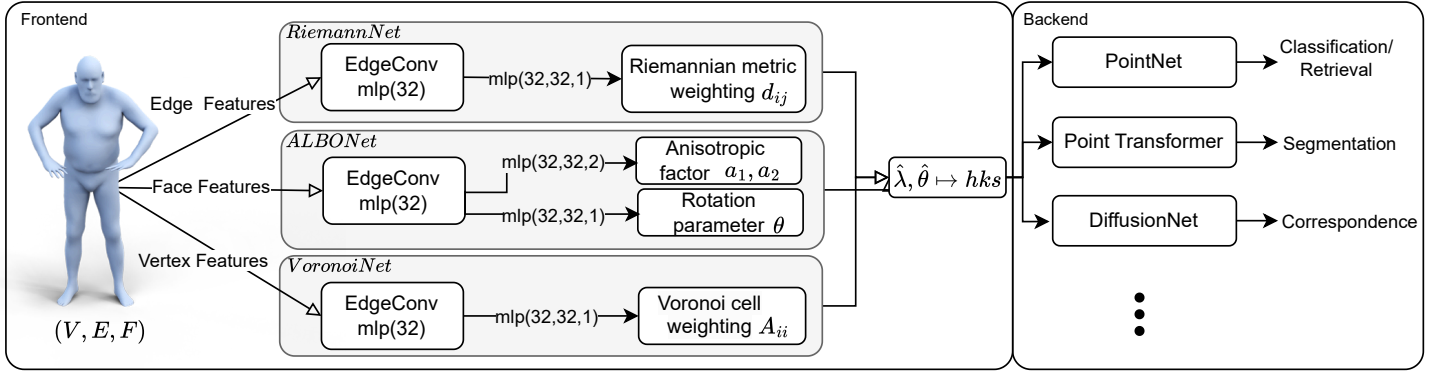


Fig. 3. **LBONet Architecture.** LBONet takes features on mesh edges, vertices, and faces as input of its three building blocks, RiemannNet and VoronoiNet. Each block consists of one EdgeConv which is creating a local neighbourhood graph as in [23] and learns an neighbourhood function. Then the features are passed through multiple shared mlps to predict either the Riemannian metric on an edge, the anisotropy on a face or the Voronoi cell weighting at a vertex. These predictions are applied directly on the discretized LBO, modifying the stiffness and mass matrix, which we detail out from subsection D onwards. Its eigenbasis is then used to form a spectral descriptor, which then can be passed into a "backend" for further processing.

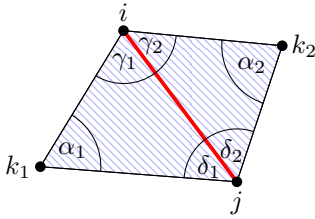


Fig. 4. Edge flap surrounding edge ij . Adjusting the Riemannian metric, which is highlighted in red, has an impact on all the angles and distances shown and are hence part of the gradients introduced.

We introduce the gradients for the mass matrix A for the module RiemannNet:

$$\frac{\partial A_{ii}}{\partial d_{ij}} = \frac{1}{8} \left(\left(-\frac{d_{ij}^3}{\sin^2(\alpha_1)2T_1} + \cot(\alpha_1)2d_{ij} \right) + \left(\frac{d_{jk}^3 \cos(\gamma_1)}{\sin^2(\delta_1)2T_1} \right) - \left(\frac{d_{ij}^3}{\sin^2(\alpha_2)2T_2} + \cot(\alpha_2)2d_{ij} \right) + \left(\frac{d_{jk}^3 \cos(\gamma_2)}{\sin^2(\delta_2)2T_2} \right) \right), \quad (19)$$

where T is the area of the triangle. As triangles have to obey the triangular inequality to be valid, specific weightings can render a triangle invalid, resulting in a failure to solve for the eigenbasis. To mitigate this, [17] proposed to use Rosen's gradient projection method [40], which projects the gradient into the search direction by taking the triangular inequality into account. As our proposed method takes a different strategy to weight the Riemannian metric, we treat it as a metric nearness problem and solve it in the forward-pass as proposed in [41]. This iterative algorithm first weights the triangle with the given weights, which might result in an invalid triangle. Then for every rotation (ijk, jki, kji) of the triangle, the violation is calculated with $d_{ik} + d_{jk} - d_{ij}$ which then is used to derive correction terms with $\frac{1}{3}(e_{ij} - e_{ik} - e_{jk})$. This corrective term is then subtracted from the violating edge term e_{ij} and is added onto the remaining edge terms (e_{ik}, e_{jk}) . This routine is repeated until no triangular inequality is violated. As collinear vertices in a triangle or triangles very close to having collinear

vertices produce exploding gradients, we add a small term ϵ to the corrective term. This results in a much smoother gradient and prevents invalid eigenbases.

E. Learning on mesh faces

ALBO was introduced by [13] and adopted in the wider literature in various neural network applications [42] [25] [43] proving the potential beyond the standard LBO. However, the increased power comes at the cost of precalculating ALBO for every combination of anisotropic factor α and angle θ . Furthermore, as both parameters are discrete, important discriminativity might lie between two discrete values and might go unused. To avoid confusion with the notation used in this paper, we label the anisotropic factors as $a_x = \alpha_x$.

As the presented work allows the propagation of a loss function through the LBO eigenbasis, we take a step further and instead of just using ALBO with its standard parameters, we learn them from given data by face-wise perceptrons. By this we can learn a powerful ALBO which is highly adaptive over the manifold, which would otherwise be very hard to obtain with traditional methods.

We adopt the approach from [13] with learning the anisotropic factor a into the principal curvature directions and the extension to the rotation parameter θ introduced later in [25]. Additionally, we extend ALBO to learn into both directions at the same time, which we term as ALBO+. Our ablation study shows that there is a significant benefit in allowing the neural network to learn in both directions.

A more general form of equation 1 can be expressed as,

$$\Delta_D f = \nabla D(\nabla f) \quad (20)$$

where D is referred to as *thermal conductivity* tensor and is defined by a 2×2 matrix and controls the direction and anisotropic level of the diffusion.

Andreux et al. [13] proposed to use a tensor based on the principal curvature directions (κ_m, κ_M) forming an orthonormal basis $V_{ijk} = (v_m, v_M)$ on mesh faces,

$$D_a = \begin{pmatrix} \psi_a^m(\kappa_m, \kappa_M) & 0 \\ 0 & \psi_a^M(\kappa_m, \kappa_M) \end{pmatrix}, \quad (21)$$

where a controls the degree of anisotropy as illustrated in red in figure 5.

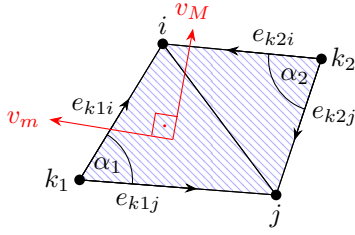


Fig. 5. Orthonormal reference frame on a face depicted by v_m and v_M based on the principal curvature directions, which is highlighted red. Scaling the directions v_m and v_M by a can change the anisotropy on the given face, which results in scaling dot product, between the corresponding edge and the direction.

Later [25] proposed to include the rotation parameter θ by rotating D_a ,

$$D_{a\theta} = R_\theta D_a(x) R_\theta^T, \quad (22)$$

where R_θ denotes the rotation matrix as illustrated red in figure 6.

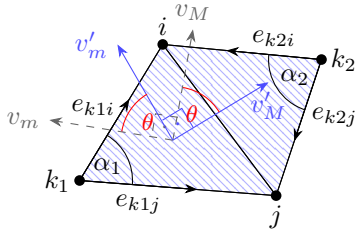


Fig. 6. Orthonormal reference frame on a face depicted by v_m and v_M based on the principal curvature directions, which is highlighted blue. It is rotated by θ , which is depicted red. Besides, scaling the directions v_m and v_M rotating the directions has a direct impact on the used dot products.

While the authors [25] fix the anisotropic factor in one direction and varying the other direction, we apply ALBO+ in all our experiments as it is more powerful than the standard ALBO.

This results in a change in the stiffness matrix W , which now is defined as:

$$W_D(i, j) = \begin{cases} \frac{\langle e_{k1j}, e_{k1i} \rangle_H}{\sin \alpha_1} + \frac{\langle e_{k2j}, e_{k2i} \rangle_H}{\sin \alpha_2}, & \text{if } (i, j) \in E \\ -\sum_{k \neq i} W(i, k), & \text{if } i = j \\ 0, & \text{otherwise,} \end{cases} \quad (23)$$

where

$$\langle e_{kj}, e_{ki} \rangle_H = e_{kj}^T \underbrace{V_{ijk} D_{a\theta} V_{ijk}^T}_H e_{ki} \quad (24)$$

and e being the respective edge on the triangle depicted in figure 6.

As the changes of equation 23 impact only the stiffness matrix W , we adjust Nelson's method given in equation 12 by omitting the gradients for the mass matrix A ,

$$\frac{\partial \lambda_k}{\partial p_{ij}} = \phi_k^T (-\lambda_k \Delta W) \phi_k, \quad (25)$$

$$F_i = \phi^T \left(\frac{\partial W_k}{\partial p_{ij}} \right) \phi A \phi - \left(\frac{\partial W_k}{\partial p_{ij}} \right) \phi \quad (26)$$

1) *Gradient sign of dot products*: The gradient of the dot product in ALBO, i.e. edge e_{k1} and v_m changes its sign, depending on which side e_{k1} is wrt. v_m . To calculate the sign, we use the product of the cross products,

$$\text{sign}(x) = e_{k1i} \times e_{k1j} * e_{k1j} \times v_m \quad (27)$$

This sign is then applied to all dot products in the ALBO to correct the sign.

2) *Anisotropic factors a_1, a_2* :

$$\frac{\partial W_{ii}}{\partial a_x} = \frac{1}{2} \langle e_{ki} v_M \rangle^2 (\cot(\alpha_1) + \cot(\alpha_2)), \quad (28)$$

where $x \in \{1, 2\}$ is the corresponding factor scaling each principal curvature direction in figure 5 and f any given face on the mesh, e.g. ijk_1 in figure 5.

3) *Rotation parameter θ* : As the rotation only occurs on the orthogonal plane formed by the principal directions (see figure 6), the problem is reduced onto the angle only and is given by:

$$\begin{aligned} \frac{\partial W_{ii}}{\partial \theta_f} = & -(\cot(\alpha_1) + \cot(\alpha_2))(a_1 \sin \cos^{-1} \langle e_{ki} v_M \rangle \langle e_{kj} v_M \rangle \\ & + a_2 \sin \cos^{-1} \langle e_{ki} v_m \rangle \langle e_{kj} v_m \rangle). \end{aligned} \quad (29)$$

4) *ALBONet and RiemannNet*: As the previously introduced RiemannNet gradients assume the LBO to be isotropic, the introduction of ALBONet requires a new set of RiemannNet gradients for the stiffness matrix for the anisotropic case,

$$\begin{aligned} \frac{\partial W_{ii}}{\partial d_{ij}} = & -\frac{1}{2} (a_1 \langle e_{ki} v_M \rangle^2 + a_2 \langle e_{ki} v_m \rangle^2) \frac{d_{ij}}{2T} \frac{1}{\sin(\delta)^2} \\ & - \frac{(d_{ik} \cos(\gamma))}{2T} \frac{1}{\sin(\alpha)^2} \\ & + (a_1 2 \sin \cos^{-1}(\langle e_{ki} v_M \rangle)) \langle e_{ki} v_M \rangle \frac{d_{ik} \cos(\gamma)}{2T} \\ & + a_2 2 \sin \cos^{-1}(\langle e_{ki} v_m \rangle) \langle e_{ki} v_m \rangle \frac{d_{ik} \cos(\gamma)}{2T} (\cot(\alpha_1) \\ & + \cot(\alpha_2)) \end{aligned} \quad (30)$$

F. Learning on mesh vertices

Weighting the Voronoi cell has been proven to be beneficial by [29] [11]. The challenge however remains in the strategy of weighting the Voronoi cell. Similar to [29], we propose to backpropagate the loss through the LBO eigenbasis but learn the Voronoi cell weighting A_{ii} by vertex-wise perceptrons instead.

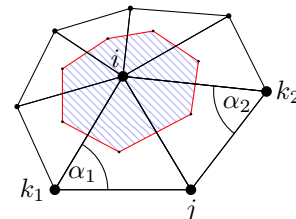


Fig. 7. Voronoi cell on vertex i , which is outlined in red. The Voronoi cell can be scaled and has only impact on the local Voronoi cell.

The changes for VoronoiNet are limited to the mass matrix A . Therefore we adjust Nelson’s method given in equation 12 by omitting the gradients for the stiffness matrix W ,

$$\frac{\partial \lambda_k}{\partial m_{ij}} = \phi_k^T (\Delta A) \phi_k, \quad (31)$$

$$F_i = \phi^T \left(-\lambda_i \frac{\partial A_k}{\partial d_{ij}} \right) \phi A \phi - \left(\lambda_i \frac{\partial A_k}{\partial d_{ij}} \right) \phi \quad (32)$$

and introduce the gradients for VoronoiNet as:

$$\frac{\partial A_{ii}}{\partial v_{ii}} = A_{ii}. \quad (33)$$

G. LBONet Architecture

Our contribution can be plugged into any recent work which we refer to as ”backend” (see figure 3), however we demonstrate in our ablation study that even with a traditional backend (a single shared mlp), LBONet is able to outperform neural networks with comprehensive backends such as [23] [44] [5]. The performance comparison to [5] is particularly interesting because our ablation proves that the performance gain obtained by PointNet++, can be similarly obtained by learning with LBONet through the LBO eigenbasis. The upside this work presents however is, that it can still be combined with a more recent backend to gain an even better performance. LBONet outperforms on many benchmarks or achieves competitive results. We show this with one backend derived from PointNet [33] for retrieval and classification. The study of pooling operations in [6] reveals that average pooling is clearly outperforming max pooling; Therefore, we apply average pooling rather than max pooling. For segmentation tasks we derive the backend from point transformer [35], by feeding the resulting spectral descriptor into the transformer and into the dimensionality reduction layer by a skip connection. Finally, for correspondence tasks we observed that the setup of DiffusionNet [7] is a great fit as it is making use of heat kernel signature and functional maps, both elements which the presented method is learning. LBONet can be combined with any backend as long as the gradients backpropagated to the spectral descriptors are useful (we observed with deep networks vanishing gradients, which we circumvented with skip connections). Furthermore to speed up learning, we implemented a routine to learn LBONet directly on the given data and then combined it with the backend for fine tuning. While it is possible to run the experiments in a single go, this approach proved to be more efficient with comparable results.

Furthermore to stabilize and increase the speed of learning features with LBONet, we employ batch normalization, after every shared mlp.

H. Implementation

a) Forward pass: We solve the generalized eigenvalue problem on the CPU using SciPy’s [45] implementation of restarted Arnoldi methods [46]. The neural networks are implemented in PyTorch [47] and are trained on a single GPU except for the correspondence task, which due its mesh resolution required to be trained on an Nvidia H100.

b) Backward pass: Standard libraries such as PyTorch or Tensorflow only allow to differentiate the full spectrum of a matrix, creating two problems: firstly the sparsity of the data is not respected, and secondly, as the most important information is contained within the lower frequencies, one cannot target specific eigenfrequencies. HodgeNet [14] takes an alternative approach to mitigate these problems. As of writing this paper, the *LOBPCG* method in PyTorch does not support backpropagation when both stiffness and mass matrix are provided, moreover it cannot deal with sparse matrices.

Vertices	1024	2048	4096
RiemannNet	0.09	0.51	3.4
ALBONet	0.05	0.4	2.5
ALBONet+	0.08	0.6	3.3
VoronoiNet	0.03	0.2	0.8

TABLE I
BACKPROPAGATION RUNTIMES ON VARYING MESH RESOLUTION ON A RTX 4090 GPU GIVEN IN SECONDS.

LBONet introduces a framework to tackle both these problems by respecting the sparsity of the data and by addressing only a certain range of frequencies (first eigenfrequencies can be skipped as they capture very global features) while differentiating the eigenbasis. We introduce custom functions to deal with sparse data and a subset of the eigenfrequencies. Despite the computational complexity, the presented routine is fully vectorized in both dimensions, edges/faces/vertices and frequencies, calculating the whole gradient of a mesh for the whole eigenbasis in one go resulting in a computation in a reasonable timeframe, see table I for the running times of the presented modules. In contrast to HodgeNet, the backpropagation procedure of LBONet does not require the computation of additional eigenfrequencies. Conversely, we observed the learning effect to be extending to frequencies, which were not used during the training process. This effect could allude that the features learnt by LBONet could generalize across frequencies as well, which is subject to further research. As the eigenbasis gradient can be very sensitive and take extreme values in certain cases we apply gradient clipping, to mediate numerical instabilities during the training process. Despite being computationally expensive to train, LBONet itself does not include many parameters, as the neural networks are all shared and relatively small. The features learned are fundamental to the manifold and therefore improvements to the standard LBO can be observed after few epochs of learning and does not require extended amount of training. Due to compactness of the network and the learned features being fundamental, the features learnt do generalize well to unseen data as our evaluation shows. We release our code to reproduce and to be incorporated in further research under <https://github.com/yioguz/LBONet>.

V. EVALUATION

We evaluate LBONet quantitatively on several experiments in the disciplines of retrieval, classification. As in the retrieval and classification tasks the goal is to learn global descriptors, we show the potency of LBONet in segmentation, and correspondence tasks which rely on descriptors with local accuracy.

For every benchmark we give the baseline results, which is achieved by completely omitting LBONet and only relying on the standard heat kernel signature. Furthermore, to illustrate the net gain of our contribution we make an ablation study on a segmentation and retrieval benchmarks by comparing standard LBO to LBONet in detail. In all experiments, we train LBONet on the first 32 eigenfrequencies and use EdgeConv with a neighbourhood size of 20 and two layers of shared mlps (32 neurons each layer) with LeakyRelu activation and batch normalization.

A. Retrieval

We report our retrieval results with the established performance metrics introduced by [48], which reward different characteristics of the search result. We evaluate our model on the SHREC’11 [49], SHREC’14 [50] and SHREC’15 benchmarks [51]. The SHREC’11 benchmark consists of 600 manifolds divided into 30 classes with 20 shapes for each class. We adapt the approach [7] by training only on 10 shapes. We repeat the experiment five times by drawing randomly different samples to train and average the results. The SHREC’14 benchmark consists of two datasets, which are obtained from real scans and synthetic manifolds. The ‘real’ benchmark especially proves itself as a real challenge in the scientific community, as algorithms fail to achieve a high accuracy on this benchmark. For SHREC’15 benchmark we adapt the approach of [5] and use k-fold cross validation to derive the performance metrics.

We achieve competitive results on SHREC’11 (table II) with perfect results. On both SHREC’14 benchmarks (tables III,IV), we outperform all other methods. Especially, the results in the ‘real’ benchmark are striking. The jump in the first tier metric demonstrates the capability of LBONet to exploit further potential from the LBO. As the dataset of SHREC’11 is a subset of SHREC’15, we see a similar performance gain on SHREC’15 (table V) with near-perfect results. It is worthy of mention that the addition of manifolds with noise and topological changes has not much of an observable deficit on the results. We elaborate on how LBONet achieves this performance gain of the heat kernel signature in the ablation study.

Method	NN	FT	ST	DCG
SD-GDM-meshSIFT [49]	100	97.20	99.01	99.55
FV-IWKS [8]	99.83	95.91	98.60	99.37
KLBO [52]	100	100	100	100
Baseline	99.67	98.04	98.30	99.11
LBONet	100	100	100	100

TABLE II
RESULTS ON SHREC’11 DATASET (IN %)

Method	NN	FT	ST	DCG
supDLtrain [2]	79.3	72.7	91.4	89.1
DeepGM [53]	72.5	53.6	82.7	78.2
SOST [6]	85.3	63.2	85.2	85.1
Baseline	85	64.81	86.03	86.41
LBONet	86.5	77.33	91.14	90.69

TABLE III
RESULTS ON SHREC’14 ‘REAL’ DATASET (IN %)

Method	NN	FT	ST	DCG
supDLtrain [2]	96.0	88.7	99.1	97.5
DeepGM [53]	99.3	81.4	98.3	96.7
3D-DL [54]	92.3	76.0	91.1	92.1
KLBO [52]	88.83	81.58	95.12	94.03
Baseline	97.33	81.40	95.25	95.30
LBONet	99.33	89.21	97.95	97.87

TABLE IV
RESULTS ON SHREC’14 ‘SYNTHETIC’ DATASET (IN %)

Method	NN	FT	ST	DCG
HAPT [9]	99.8	96.6	98.2	99.2
DeepGM [53]	99.3	94.0	97.2	98.8
AP-SOST-Net [6]	99.1	93.7	96.5	97.5
KLBO [52]	99.92	98.59	99.33	99.59
Baseline	97.2	96.4	98.5	98.48
LBONet	99.20	98.80	99.70	99.48

TABLE V
RESULTS ON SHREC’15 DATASET (IN %)

B. Classification

In order to compare the presented work to the broader literature, we conduct the experiments on SHREC’11 and SHREC’15 in a classification setting. Therefore we employ the same settings as in the retrieval case, with the exception of using cross entropy loss for learning.

We observe a similar performance gain as in the retrieval case for both benchmarks. The accuracy for SHREC’11 (table VI) and on SHREC’15 (table VII) is perfect. We observed that after applying LBONet that near-isometries are alleviated to some extent as demonstrated in figure 8.

Method	Accuracy
MeshCNN [44]	91.0
HodgeNet [14]	94.67
MeshWalker [55]	97.1
PD-MeshNet [56]	99.1
FC [57]	99.2
DiffusionNet [7]	99.7
Baseline	98.0
LBONet	100.0

TABLE VI
RESULTS ON SHREC’11 DATASET (IN %)

Method	Accuracy
DeepGM [53]	93.03
SpiderCNN [58]	95.8
PointNet++ [5]	96.09
Baseline	97.8
LBONet	100.0

TABLE VII
RESULTS ON SHREC’15 DATASET (IN %)

C. Segmentation

Segmentation has become an important task and challenging benchmarks such as the human segmentation benchmark remain hard. As recent works got better in solving them as compared to traditional methods, it is interesting to measure

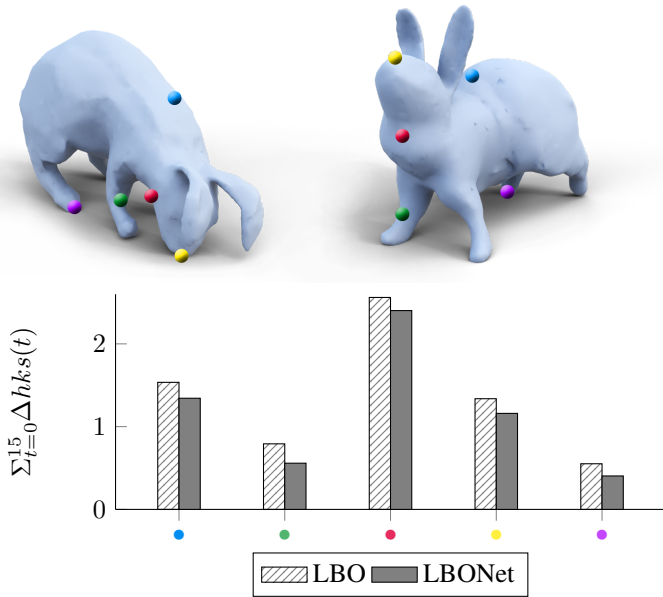


Fig. 8. Heat kernel signature at selected points evaluated with the standard LBO and with the LBONet trained on the SHREC11 benchmark. Values are given as the difference of the heat kernel at the highlighted points.

the gain of the presented work, as most spectral based methods have been outperformed recently. To measure the increase of the accuracy of local descriptors and the impact of LBONet, we run experiments on four established segmentation benchmarks. The humans segmentation benchmark [59] has been used widely across the literature and features human shapes in different poses, which we will be referred as humans in the following. The COSEG benchmarks [60] feature vases, chairs, and aliens, which we indicate in the following by their category. As backend we use a modified version of [35], where we use skip connections to allow better gradient flow into LBONet. We evaluate on the humans test set and for the COSEG benchmarks, we adapt the training setup as in [44] [56] [14] and split the dataset randomly in 85% for training, and 15% for testing. We report our results based on hard labels in table VIII. We outperform most of the methods,

Method	Humans	Vases	Chairs	Aliens
MeshCNN [44]	85.4	92.36	92.99	96.26
HodgeNet [14]	85.0	90.30	95.68	96.03
PD-MeshNet [56]	85.6	95.36	97.23	98.18
DGCNN [23]	89.7	-	-	-
DiffusionNet [7]	91.7	-	-	-
MeshWalker [55]	92.7	-	-	-
FC [57]	92.9	-	-	-
Baseline	91.1	94.7	96.5	97.2
LBONet	92.7	95.6	97.8	98.3

TABLE VIII

SEGMENTATION ACCURACY ON HUMANS AND COSEG BENCHMARKS (IN %)

including DiffusionNet and MeshCNN. All other methods were already outperformed by the simple architecture used in our ablation study (table X) and when LBONet is combined with a recent backend such as a point transformer [35], it

becomes even more powerful as the learning can be based on a highly optimized spectral descriptor provided by LBONet. For a fair comparison we also include the performance of our baseline method [35] based on the standard heat kernel signature and the net gain of using LBONet becomes apparent. We discuss the effects of LBONet to the LBO eigenbasis in the segmentation tasks in the ablation study, which further reveals how the segments of the manifolds become “encoded” into the LBO eigenbasis, making it easier for descriptors to separate the segments more easily.

D. Functional Correspondence

For functional correspondence tasks we adapt the supervised setup from [7] for the FAUST [61] dataset. The FAUST dataset includes both intra- and interclass manifolds of varying degree of near-isometric deformation for training and testing. It serves as a great way to compare the performance gain with the wider literature. We randomly generate all combinations of the 80 manifolds for training and test on the remaining combinations of 20 manifolds. The errors are averaged over all manifolds. We learn the eigenbasis through the heat kernel signature directly using triplet loss using corresponding points and generating dissimilar points on the fly. We feed the learned heat kernel signature and its eigenbasis into DiffusionNet and achieve a significant reduction in geodesic mean error, proving two facts, first that the learned heat kernel signature is more descriptive than the standard used by DiffusionNet and second, that the eigenbasis is better for constructing functional maps after the learning.

KPConv [62]	2.9
HSN [63]	3.3
ACSCNN [28]	2.7
DiffusionNet [†] [7]	2.5
Unsupervised [64]	1.5
LBONet	1.4

TABLE IX

RESULTS ON THE FAUST [61] BENCHMARK. VALUES ARE GIVEN IN GEODESIC MEAN ERROR X 100. RESULT MARKED WITH [†]SERVES AS THE BASELINE METHOD.

In the texture transfer illustration in figure 9, one can observe that LBONet is performing the best in the areas where the stretching occurs (top row: legs, bottom row: armpits), where DiffusionNet and Unsupervised perform significantly worse. Two minor glitches are visible with LBONet. The patches are not as straight as in the ground-truth and the left forearm has some misalignment. Nevertheless, LBONet outperforms Unsupervised and correctly recognizes stretched areas.

E. Ablation Study

To prove the effectiveness of LBONet, we repeat the human segmentation [59] experiment in a more traditional setting. We conduct the experiment by using the spectral descriptor directly (see figure 3 Frontend) with a single shared mlp instead of a Backend. This way it is down to the bare minimum and we can measure LBONets contribution almost

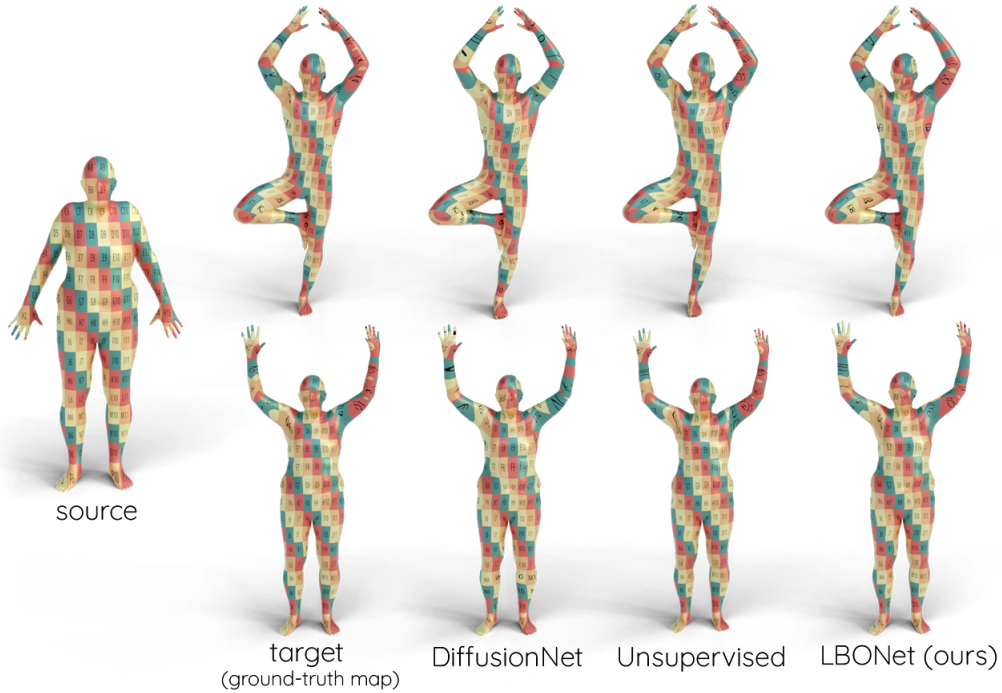


Fig. 9. Texture transfer experiment on the FAUST test set. Source illustrates the texture applied to the source shape, and target the texture mapped via the ground-truth correspondence to the target shape. Followed by the illustrations of the predictions of DiffusionNet, Unsupervised, and LBONet.

in isolation. Table X shows the results of each layer. Several observations can be made. VoronoiNet on its own does not provide much benefit, however when run in combination of the other networks such as RiemannNet or ALBONet it creates a synergistic effect. RiemannNet and ALBONet seems to have some overlapping effect as they still add some performance, however the performance gain diminishes. The most intriguing effect however is, that when ALBO is allowed to learn the anisotropic factor in both directions (ALBO+), we see a substantial increase in performance, which in the literature and methods using ALBO went mostly unnoticed. ALBO requires much higher weights to achieve the performance gain below, which ALBO+ manages to achieve with much lower weights, allowing it to influence anisotropy, without affecting the generalization. Furthermore, the increased weights with ALBO might be interfering with RiemannNet.

RiemannNet	ALBONet	ALBO+Net	VoronoiNet	Accuracy	Improvement
-	-	-	-	84.1	
-	-	-	x	84.6	0.6%
-	x	-	-	85.6	1.78%
x	-	-	-	86.9	3.33%
-	x	-	x	87.6	4.16%
x	x	-	-	87.8	4.40%
-	-	x	-	88.1	4.76%
x	-	-	x	88.1	4.76%
x	x	-	x	88.3	4.99%
x	-	x	-	89.1	5.95%
-	-	x	x	89.9	6.90%
x	-	x	x	90.7	7.85%

TABLE X

RESULTS ON HUMAN SEGMENTATION BENCHMARK. PERFORMANCES OF THE INTRODUCED MODULES WHEN COMBINED AND IN SEPARATION.

To further understand how LBONet is learning in a specific task, we visualize the learned features in a segmentation task in figure 10. At this point it is important to differentiate

that LBONet can be used with any spectral descriptor, but when used with the heat kernel signature, the spectrum will be optimized wrt. to what the signature picks out from the eigenbasis. Hence, in a correspondence task we can expect the eigenbasis to be closer after learning with LBONet, however in a segmentation task that is not necessarily the case, as LBONet will learn an eigenbasis which allows better separation of segments. As interpretation of learned features within a neural network is a difficult task and might not always yield to explainable results, some patterns are evident in figure 10. This becomes clear when considering the ground-truth segmentation. Firstly, when observing the legs, we see that ALBONet reduces the anisotropic factor into the maximum curvature direction and applies some rotation, which acts as a boundary in the spectral space between the torso and the leg. Secondly, we see a high activity on the head with RiemannNet and VoronoiNet, which both enlarge the head in the spectral space. By enlarging the head in the spectral space, the head is becoming easier to distinguish from the torso and upper arm. Lastly, we see scattered detections of further boundaries, which help to separate the segments even more. The t-SNE [65] method allows to visualize high-dimensional data in lower dimensions. By this, we can compare the standard heat kernel signature and the LBONet heat kernel signature. We visualize randomly sampled points of the signature on the test set colored by their ground-truth labels, which can be observed in figure 11. Several observations can be made from the distribution of the features and aligns with the hypothesis made earlier. We can observe that the standard LBO misclassifies lots of head parts either as torso or even as upper arms, which LBONet is able to eliminate completely. The overlap between the torso and the leg is reduced by LBONet significantly, only allowing a small part to overlap. Furthermore, we see that each

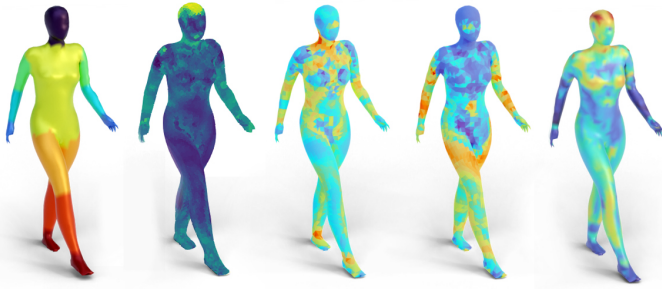


Fig. 10. Ground-truth segmentation of a manifold and learned features on a test manifold from the human segmentation benchmark by RiemannNet (second), ALBONet (third and fourth), and VoronoiNet (fifth). Interesting patterns emerge along the segmentation boundaries, which demonstrates that individual modules are stronger in certain aspects.

segment boundary has been narrowed down drastically, which allows easy separation of segments in the spectral space, which with the standard LBO seems like a hard task.

To understand the gain in a retrieval task we compare the standard heat kernel signature to the LBONet heat kernel signature by average pooling. The performance is plotted in figure 12 alongside their performance achieved in the experiment III and IV. One can observe that the performance gain in the final experiment was due to LBONet as the heat kernel signature with LBONet performs better than the standard heat kernel signature and that this performance gain translates into the final result. Similar to the ablation done in the segmentation task, we can observe that the LBONet heat kernel signature is far more descriptive.

VI. CONCLUSION

We have introduced a framework, which allows to adapt the LBO eigenbasis to the task at hand without precalculating LBO. The modules RiemannNet, ALBONet and VoronoiNet are capable of learning powerful features and add provably value to the descriptiveness of spectral descriptors. The experiments demonstrated that LBONet is versatile and can make the LBO robust against near-isometries and help to separate segments in spectral space. Moreover, we have addressed the problem of scalability, which remains still a relevant topic for future research.

VII. FUTURE WORK

Future research could incorporate further modules or explore other utilizations such as isospectralization. Another module could be incorporated to LBONet based on the recently introduced FLBO [26], allowing it to learn asymmetries on the manifold. Further research could be done on the scalability, as the backpropagation still involves some calculations of large non-sparse matrices, limiting the presented work to be run on very large meshes.

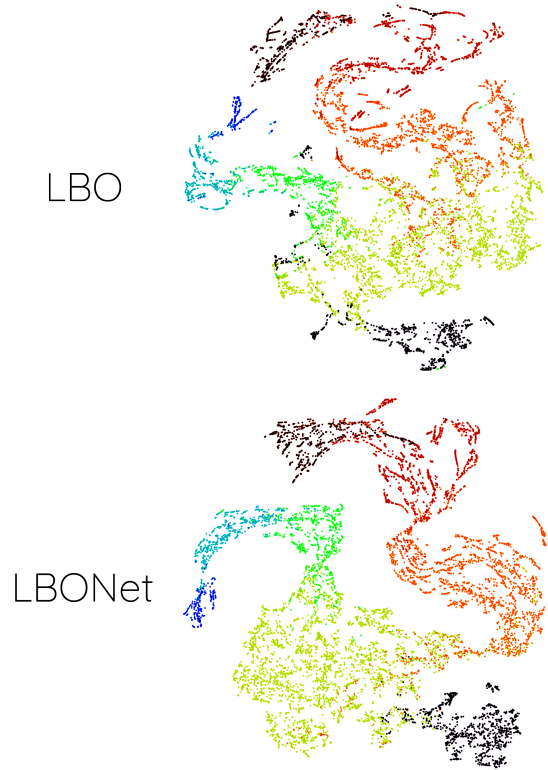


Fig. 11. Heat kernel signature features obtained from the ablation study done in chapter 5. Top shows the heat kernel signature evaluated with the standard LBO and bottom the heat kernel signature evaluated with LBONet. The features were reduced from 16 dimensions to 2D with t-SNE.

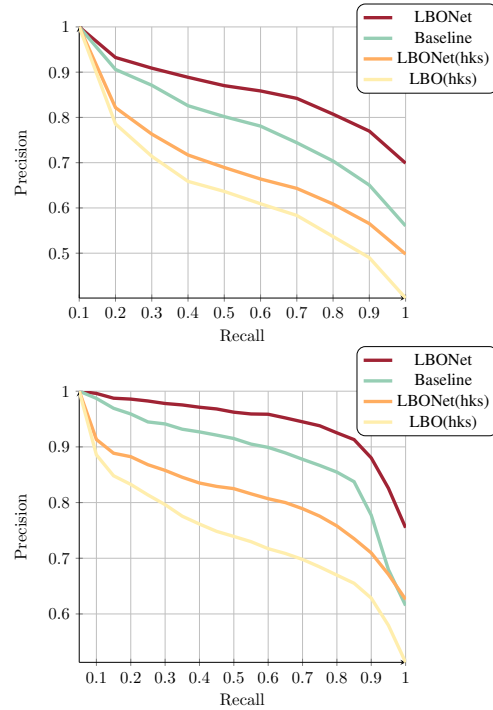


Fig. 12. Precision/Recall curve of LBONet, Baseline, LBONet hks, and the LBO hks evaluated on the SHREC'14 'real' benchmark (top) and SHREC'14 'synthetic' benchmark (bottom). Distances were calculated using Euclidean distance. The performance of the spectral signatures for both LBONet (hks) and LBO (hks) were determined by using average pooling.

REFERENCES

- [1] I. Kokkinos, M. M. Bronstein, R. Litman, and A. M. Bronstein, "Intrinsic shape context descriptors for deformable shapes," in *2012 IEEE Conference on Computer Vision and Pattern Recognition*. IEEE, 2012, pp. 159–166.
- [2] R. Litman, A. Bronstein, M. Bronstein, and U. Castellani, "Supervised learning of bag-of-features shape descriptors using sparse coding," in *Computer Graphics Forum*, vol. 33, no. 5. Wiley Online Library, 2014, pp. 127–136.
- [3] J. Masci, D. Boscaini, M. Bronstein, and P. Vanderghyest, "Shapenet: Convolutional neural networks on non-euclidean manifolds," Tech. Rep., 2015.
- [4] L. Yi, H. Su, X. Guo, and L. J. Guibas, "Syncspecnn: Synchronized spectral cnn for 3d shape segmentation," in *Proceedings of the IEEE Conference on Computer Vision and Pattern Recognition*, 2017, pp. 2282–2290.
- [5] C. R. Qi, L. Yi, H. Su, and L. J. Guibas, "Pointnet++: Deep hierarchical feature learning on point sets in a metric space," in *Advances in neural information processing systems*, 2017, pp. 5099–5108.
- [6] R. Yu, J. Sun, and H. Li, "Second-order spectral transform block for 3d shape classification and retrieval," *IEEE Transactions on Image Processing*, vol. 29, pp. 4530–4543, 2020.
- [7] N. Sharp, S. Attaiki, K. Crane, and M. Ovsjanikov, "Diffusionnet: Discretization agnostic learning on surfaces," *ACM Transactions on Graphics (TOG)*, vol. 41, no. 3, pp. 1–16, 2022.
- [8] F. A. Limberger and R. C. Wilson, "Feature encoding of spectral signatures for 3d non-rigid shape retrieval."
- [9] A. Giachetti and C. Lovato, "Radial symmetry detection and shape characterization with the multiscale area projection transform," in *Computer graphics forum*, vol. 31, no. 5. Wiley Online Library, 2012, pp. 1669–1678.
- [10] J. Ye, Z. Yan, and Y. Yu, "Fast nonrigid 3d retrieval using modal space transform," in *Proceedings of the 3rd ACM conference on International conference on multimedia retrieval*, 2013, pp. 121–126.
- [11] F. A. Limberger and R. C. Wilson, "Curvature-based spectral signatures for non-rigid shape retrieval," *Computer Vision and Image Understanding*, vol. 172, pp. 1–11, 2018.
- [12] Y. Choukroun, A. Shtern, A. Bronstein, and R. Kimmel, "Hamiltonian operator for spectral shape analysis," *IEEE transactions on visualization and computer graphics*, vol. 26, no. 2, pp. 1320–1331, 2018.
- [13] M. Andreux, E. Rodola, M. Aubry, and D. Cremers, "Anisotropic laplace-beltrami operators for shape analysis," in *Computer Vision-ECCV 2014 Workshops: Zurich, Switzerland, September 6-7 and 12, 2014, Proceedings, Part IV 13*. Springer, 2015, pp. 299–312.
- [14] D. Smirnov and J. Solomon, "Hodgenet: Learning spectral geometry on triangle meshes," *ACM Transactions on Graphics (TOG)*, vol. 40, no. 4, pp. 1–11, 2021.
- [15] M. Reuter, F.-E. Wolter, and N. Peinecke, "Laplace-spectra as fingerprints for shape matching," in *Proceedings of the 2005 ACM symposium on Solid and physical modeling*. ACM, 2005, pp. 101–106.
- [16] M. Meyer, M. Desbrun, P. Schröder, and A. H. Barr, "Discrete differential-geometry operators for triangulated 2-manifolds," in *Visualization and mathematics III*. Springer, 2003, pp. 35–57.
- [17] J. K. Gahm, Y. Shi, A. D. N. Initiative *et al.*, "Riemannian metric optimization on surfaces (rms) for intrinsic brain mapping in the laplace-beltrami embedding space," *Medical image analysis*, vol. 46, pp. 189–201, 2018.
- [18] R. M. Rostamov, "Laplace-beltrami eigenfunctions for deformation invariant shape representation," in *Proceedings of the fifth Eurographics symposium on Geometry processing*. Eurographics Association, 2007, pp. 225–233.
- [19] J. Sun, M. Ovsjanikov, and L. Guibas, "A concise and provably informative multi-scale signature based on heat diffusion," in *Computer graphics forum*, vol. 28, no. 5. Wiley Online Library, 2009, pp. 1383–1392.
- [20] M. M. Bronstein and I. Kokkinos, "Scale-invariant heat kernel signatures for non-rigid shape recognition," in *2010 IEEE Computer Society Conference on Computer Vision and Pattern Recognition*. IEEE, 2010, pp. 1704–1711.
- [21] S. E. Naffouti, Y. Fougere, I. Aouissou, A. Sakly, and F. Mériaudeau, "Heuristic optimization-based wave kernel descriptor for deformable 3d shape matching and retrieval," *Signal, Image and Video Processing*, vol. 12, no. 5, pp. 915–923, 2018.
- [22] R. Litman and A. M. Bronstein, "Learning spectral descriptors for deformable shape correspondence," *IEEE transactions on pattern analysis and machine intelligence*, vol. 36, no. 1, pp. 171–180, 2013.
- [23] Y. Wang, Y. Sun, Z. Liu, S. E. Sarma, M. M. Bronstein, and J. M. Solomon, "Dynamic graph cnn for learning on point clouds," *Acm Transactions On Graphics (tog)*, vol. 38, no. 5, pp. 1–12, 2019.
- [24] D. Boscaini, J. Masci, S. Melzi, M. M. Bronstein, U. Castellani, and P. Vanderghyest, "Learning class-specific descriptors for deformable shapes using localized spectral convolutional networks," in *Computer Graphics Forum*, vol. 34, no. 5. Wiley Online Library, 2015, pp. 13–23.
- [25] D. Boscaini, J. Masci, E. Rodolà, M. M. Bronstein, and D. Cremers, "Anisotropic diffusion descriptors," in *Computer Graphics Forum*, vol. 35, no. 2. Wiley Online Library, 2016, pp. 431–441.
- [26] S. Weber, T. Dagès, M. Gao, and D. Cremers, "Finsler-laplace-beltrami operators with application to shape analysis," *arXiv preprint arXiv:2404.03999*, 2024.
- [27] L. Cosmo, M. Panine, A. Rampini, M. Ovsjanikov, M. M. Bronstein, and E. Rodola, "Isospectralization, or how to hear shape, style, and correspondence," in *Proceedings of the IEEE/CVF conference on computer vision and pattern recognition*, 2019, pp. 7529–7538.
- [28] A. Rampini, I. Tallini, M. Ovsjanikov, A. M. Bronstein, and E. Rodola, "Correspondence-free region localization for partial shape similarity via hamiltonian spectrum alignment," in *2019 International Conference on 3D Vision (3DV)*. IEEE, 2019, pp. 37–46.
- [29] Y. Shi, R. Lai, R. Gill, D. Pelletier, D. Mohr, N. Sicotte, and A. W. Toga, "Conformal metric optimization on surface (cmos) for deformation and mapping in laplace-beltrami embedding space," in *International Conference on Medical Image Computing and Computer-Assisted Intervention*. Springer, 2011, pp. 327–334.
- [30] M. Ovsjanikov, M. Ben-Chen, J. Solomon, A. Butscher, and L. Guibas, "Functional maps: a flexible representation of maps between shapes," *ACM Transactions on Graphics (ToG)*, vol. 31, no. 4, pp. 1–11, 2012.
- [31] M. Aubry, U. Schlickewei, and D. Cremers, "The wave kernel signature: A quantum mechanical approach to shape analysis," in *2011 IEEE international conference on computer vision workshops (ICCV workshops)*. IEEE, 2011, pp. 1626–1633.
- [32] L. Cosmo, G. Minello, M. Bronstein, E. Rodolà, L. Rossi, and A. Torsello, "3d shape analysis through a quantum lens: the average mixing kernel signature," *International Journal of Computer Vision*, vol. 130, no. 6, pp. 1474–1493, 2022.
- [33] C. R. Qi, H. Su, K. Mo, and L. J. Guibas, "Pointnet: Deep learning on point sets for 3d classification and segmentation," in *Proceedings of the IEEE conference on computer vision and pattern recognition*, 2017, pp. 652–660.
- [34] M.-H. Guo, J.-X. Cai, Z.-N. Liu, T.-J. Mu, R. R. Martin, and S.-M. Hu, "Pct: Point cloud transformer," *Computational Visual Media*, vol. 7, pp. 187–199, 2021.
- [35] H. Zhao, L. Jiang, J. Jia, P. H. Torr, and V. Koltun, "Point transformer," in *Proceedings of the IEEE/CVF international conference on computer vision*, 2021, pp. 16259–16268.
- [36] C.-C. Wong, "Heat diffusion based multi-scale and geometric structure-aware transformer for mesh segmentation," in *Proceedings of the IEEE/CVF Conference on Computer Vision and Pattern Recognition*, 2023, pp. 4413–4422.
- [37] S. Rusinkiewicz, "Estimating curvatures and their derivatives on triangle meshes," in *Proceedings. 2nd International Symposium on 3D Data Processing, Visualization and Transmission, 2004. 3DPVT 2004*. IEEE, 2004, pp. 486–493.
- [38] S. Tang and A. Godil, "An evaluation of local shape descriptors for 3d shape retrieval," in *Three-Dimensional Image Processing (3DIP) and Applications II*, vol. 8290. International Society for Optics and Photonics, 2012, p. 82900N.
- [39] R. B. Nelson, "Simplified calculation of eigenvector derivatives," *AIAA journal*, vol. 14, no. 9, pp. 1201–1205, 1976.
- [40] J. B. Rosen, "The gradient projection method for nonlinear programming, part i. linear constraints," *Journal of the society for industrial and applied mathematics*, vol. 8, no. 1, pp. 181–217, 1960.
- [41] I. S. Dhillon, S. Sra, and J. A. Tropp, "Triangle fixing algorithms for the metric nearness problem," in *NIPS*, 2004, pp. 361–368. [Online]. Available: <http://papers.nips.cc/paper/2598-triangle-fixing-algorithms-for-the-metric-nearness-problem>
- [42] D. Boscaini, J. Masci, E. Rodolà, and M. Bronstein, "Learning shape correspondence with anisotropic convolutional neural networks," *Advances in neural information processing systems*, vol. 29, 2016.
- [43] Q. Li, S. Liu, L. Hu, and X. Liu, "Shape correspondence using anisotropic chebyshev spectral cnns," in *Proceedings of the IEEE/CVF conference on Computer Vision and Pattern Recognition*, 2020, pp. 14 658–14 667.

- [44] R. Hanocka, A. Hertz, N. Fish, R. Giryas, S. Fleishman, and D. Cohen-Or, "Meshcnn: a network with an edge," *ACM Transactions on Graphics (TOG)*, vol. 38, no. 4, pp. 1–12, 2019.
- [45] P. Virtanen, R. Gommers, T. E. Oliphant, M. Haberland, T. Reddy, D. Cournapeau, E. Burovski, P. Peterson, W. Weckesser, J. Bright, S. J. van der Walt, M. Brett, J. Wilson, K. J. Millman, N. Mayorov, A. R. J. Nelson, E. Jones, R. Kern, E. Larson, C. J. Carey, Í. Polat, Y. Feng, E. W. Moore, J. VanderPlas, D. Laxalde, J. Perktold, R. Cimrman, I. Henriksen, E. A. Quintero, C. R. Harris, A. M. Archibald, A. H. Ribeiro, F. Pedregosa, P. van Mulbregt, and S. 1.0 Contributors, "Scipy 1.0: fundamental algorithms for scientific computing in python," *Nature Methods*, vol. 17, no. 3, pp. 261–272, Mar 2020. [Online]. Available: <https://doi.org/10.1038/s41592-019-0686-2>
- [46] R. B. Lehoucq, D. C. Sorensen, and C. Yang, *ARPACK users' guide: solution of large-scale eigenvalue problems with implicitly restarted Arnoldi methods*. SIAM, 1998.
- [47] A. Paszke, S. Gross, F. Massa, A. Lerer, J. Bradbury, G. Chanan, T. Killeen, Z. Lin, N. Gimelshein, L. Antiga *et al.*, "Pytorch: An imperative style, high-performance deep learning library," *Advances in neural information processing systems*, vol. 32, 2019.
- [48] P. Shilane, P. Min, M. Kazhdan, and T. Funkhouser, "The princeton shape benchmark," in *Proceedings Shape Modeling Applications, 2004*. IEEE, 2004, pp. 167–178.
- [49] Z. Lian, A. Godil, B. Bustos, M. Daoudi, J. Hermans, S. Kawamura, Y. Kurita, G. Lavoua, P. D. Suetens *et al.*, "Shape retrieval on non-rigid 3d watertight meshes," in *Eurographics workshop on 3d object retrieval (3DOR)*. Citeseer, 2011.
- [50] D. Pickup, X. Sun, P. L. Rosin, R. Martin, Z. Cheng, Z. Lian, M. Aono, A. B. Hamza, A. Bronstein, M. Bronstein *et al.*, "Shrec'14 track: Shape retrieval of non-rigid 3d human models," in *Proceedings of the 7th Eurographics workshop on 3D Object Retrieval*, vol. 1, no. 2. Eurographics Association, 2014, p. 6.
- [51] Z. Lian, J. Zhang, S. Choi, H. ElNaghy, J. El-Sana, T. Furuya, A. Giachetti, R. A. Guler, L. Lai, C. Li, H. Li, F. A. Limberger, R. Martin, R. U. Nakanishi, A. P. Neto, L. G. Nonato, R. Ohbuchi, K. Pevzner, D. Pickup, P. Rosin, A. Sharf, L. Sun, X. Sun, S. Tari, G. Unal, and R. C. Wilson, "Non-rigid 3d shape retrieval," in *Proceedings of the 2015 Eurographics Workshop on 3D Object Retrieval*, ser. 3DOR '15. Goslar, DEU: Eurographics Association, 2015, p. 107–120.
- [52] F. A. Limberger, "Spectral signatures for non-rigid 3d shape retrieval," Ph.D. dissertation, University of York, 2017.
- [53] L. Luciano and A. B. Hamza, "A global geometric framework for 3d shape retrieval using deep learning," *Computers & Graphics*, vol. 79, pp. 14–23, 2019.
- [54] S. Bu, Z. Liu, J. Han, J. Wu, and R. Ji, "Learning high-level feature by deep belief networks for 3-d model retrieval and recognition," *IEEE Transactions on Multimedia*, vol. 16, no. 8, pp. 2154–2167, 2014.
- [55] A. Lahav and A. Tal, "Meshwalker: Deep mesh understanding by random walks," *ACM Transactions on Graphics (TOG)*, vol. 39, no. 6, pp. 1–13, 2020.
- [56] F. Milano, A. Loquercio, A. Rosinol, D. Scaramuzza, and L. Carlone, "Primal-dual mesh convolutional neural networks," *Advances in Neural Information Processing Systems*, vol. 33, pp. 952–963, 2020.
- [57] T. W. Mitchel, V. G. Kim, and M. Kazhdan, "Field convolutions for surface cnns," in *Proceedings of the IEEE/CVF International Conference on Computer Vision*, 2021, pp. 10001–10011.
- [58] Y. Xu, T. Fan, M. Xu, L. Zeng, and Y. Qiao, "Spidercnn: Deep learning on point sets with parameterized convolutional filters," in *Proceedings of the European Conference on Computer Vision (ECCV)*, 2018, pp. 87–102.
- [59] H. Maron, M. Galun, N. Aigerman, M. Trope, N. Dym, E. Yumer, V. G. Kim, and Y. Lipman, "Convolutional neural networks on surfaces via seamless toric covers," *ACM Trans. Graph.*, vol. 36, no. 4, pp. 71–1, 2017.
- [60] Y. Wang, S. Asafi, O. Van Kaick, H. Zhang, D. Cohen-Or, and B. Chen, "Active co-analysis of a set of shapes," *ACM Transactions on Graphics (TOG)*, vol. 31, no. 6, pp. 1–10, 2012.
- [61] F. Bogo, J. Romero, M. Loper, and M. J. Black, "Faust: Dataset and evaluation for 3d mesh registration," in *Proceedings of the IEEE conference on computer vision and pattern recognition*, 2014, pp. 3794–3801.
- [62] H. Thomas, C. R. Qi, J.-E. Deschaud, B. Marcotegui, F. Goulette, and L. J. Guibas, "Kpconv: Flexible and deformable convolution for point clouds," in *Proceedings of the IEEE/CVF international conference on computer vision*, 2019, pp. 6411–6420.
- [63] K. H. Ruben Wiersma, Elmar Eisemann, "Cnns on surfaces using rotation-equivariant features," *Transactions on Graphics*, vol. 39, no. 4, Jul. 2020.
- [64] D. Cao, P. Roetzer, and F. Bernard, "Unsupervised learning of robust spectral shape matching," *arXiv preprint arXiv:2304.14419*, 2023.
- [65] L. Van der Maaten and G. Hinton, "Visualizing data using t-sne." *Journal of machine learning research*, vol. 9, no. 11, 2008.